Silver Growth on TiO_2(110) (1 × 1) and (1 × 2)†

K. Luo, T. P. St. Clair, X. Lai, and D. W. Goodman*

Department of Chemistry, Texas A&M University, P.O. Box 30012, College Station, Texas 77842-3012

Received: August 26, 1999; In Final Form: November 4, 1999

The growth and interaction of Ag with the TiO_2(110) (1 × 1) and (1 × 2) surfaces were studied by X-ray photoemission spectroscopy (XPS), low-energy ion scattering (LEIS), low-energy electron diffraction (LEED), and scanning tunneling microscopy (STM). At 300 K, both LEIS and STM data indicate that Ag grows three-dimensionally on the (1 × 1) and (1 × 2) surfaces; no strong chemical interaction between Ag and TiO_2 was detected by XPS. At 0.05 ML Ag exposure (corresponding to a cluster diameter of 2.0−3.5 nm), the Ag 3d core level binding energy shifts to 1.2 eV higher than that for metallic (bulk) Ag. In addition, the Ag 3d peak width increases with decreasing cluster size. The binding energy shifts and peak broadening are attributed to both initial and final state effects. The valence band as a function of Ag exposure suggests that a metal-to-nonmetal transition occurs within the Ag clusters at exposures between 0.5 and 1 ML (3.5−4.4 nm). No change in the cluster growth mode was observed upon Ag deposition onto an Ar ion-bombarded TiO_2 surface. Also no strong interaction was observed between substrate Ti^{3+} states (induced via ion bombardment) and the Ag clusters. Significant sintering of the Ag clusters was observed upon annealing from 100 to 300 K.

Introduction

Oxide−supported metal clusters are of great interest because the structural, chemical, and electronic properties of the metal oxide interface directly affect the optimum utilization of transition metal catalysts, ceramics, and photovoltaic devices. Much of the recent related work has been summarized in several review articles.[1−8] The growth of metals on ordered TiO_2 has been studied in great depth because of the potential of titania supported metals as catalysts for a variety of reactions. Most of these studies have focused on rutile TiO_2(110).

Single-crystal TiO_2(110) has been widely used as a metal oxide support for the study of metal growth because this surface is nonpolar, thermally stable, and reducible. The surface structure and electronic properties of the TiO_2(110) (1 × 1) and (1 × 2) reconstructed surfaces have been thoroughly studied with various surface sensitive techniques, including ultraviolet photoemission spectroscopy (UPS),[9,10] X-ray photoemission spectroscopy (XPS),[11−13] electron energy loss spectroscopy (EELS),[14−16] low-energy electron diffraction (LEED),[17−20] and scanning tunneling microscopy (STM).[21−24] For metal growth on TiO_2(110), the (1 × 2) surface has been studied to a lesser extent than the (1 × 1) surface. However, metal deposition on the relatively rough (1 × 2) surface could very well lead to a variation in metal nucleation and growth kinetics compared to the (1 × 1) surface. On both surfaces, surface defects likely serve as nucleation centers for metal growth.

Silver catalysts are important for ethylene epoxidation and methanol oxidation. Ag on Al_2O_3 has been studied extensively;[25−27] however, Ag on TiO_2(110) has received much less attention. Atomic force microscopy (AFM) and XPS results were reported by D. Martin et al.[28] and D. Abriou et al.,[29] and a limited STM study was reported by X. Lai et al.[30] In this study, STM, low-energy ion scattering spectroscopy (LEIS) and LEED have been used to investigate the nucleation and growth of Ag on the TiO_2(110) (1 × 1) and (1 × 2) surfaces. XPS was employed to study the interfacial reactivity and the electronic properties of this system. In addition, LEIS and XPS were used to study the effect of temperature on the growth of Ag clusters.

Experimental Section

The first of two ultrahigh vacuum (UHV) systems used in these studies was equipped with XPS, Auger electron spectroscopy (AES), LEIS, LEED, and temperature-programmed desorption (TPD) and achieved a base pressure of ca. 5×10^{-10} Torr. The TiO_2(110) single crystal was mounted onto a molybdenum sample holder and supported by high-purity tantalum wires. The sample could be heated to 1500 K by resistive heating (to 2400 K by e-beam heating) and cooled via a liquid nitrogen reservoir attached to the copper leads. The sample temperature was measured using a W-5% Re/W-26% Re thermocouple spot-welded to the sample holder intimate to the sample but not attached directly to it. The sample was annealed to 1000 K for several hours in UHV, yielding a reduced and thus conducting sample. The stoichiometric TiO_2(110) (1 × 1) surface was prepared by Ar ion bombardment (2 kV), followed by annealing to 1000 K in 4×10^{-6} Torr of O_2 for 10 min.[31] The TiO_2(110) (1 × 2) reconstructed surface was prepared by annealing to 1300 K; both structures were verified by LEED and STM. In addition, XPS shows a small Ti^{3+} shoulder from the (1 × 2) surface due to the surface reconstruction.[13]

The Ag doser consisted of a high-purity Ag wire (99.99%) wrapped around a Ta filament, which was melted and thoroughly degassed prior to use. The Ag dosing rate, calibrated via TPD and AES using a Re(0001) substrate, was adjusted to ∼1 equivalent monolayer (ML)/360 s (where 1 ML is defined as $1.39 \times 10^{15} cm^{-2}$).

The XPS data were collected using a Mg Kα source (Perkin-Elmer) and a concentric hemispherical analyzer (PHI, SCA 10-

* To whom correspondence should be addressed.
† Part of the special issue "Gabor Somorjai Festschrift".

10.1021/jp993062o CCC: $19.00
Published on Web 12/31/1999

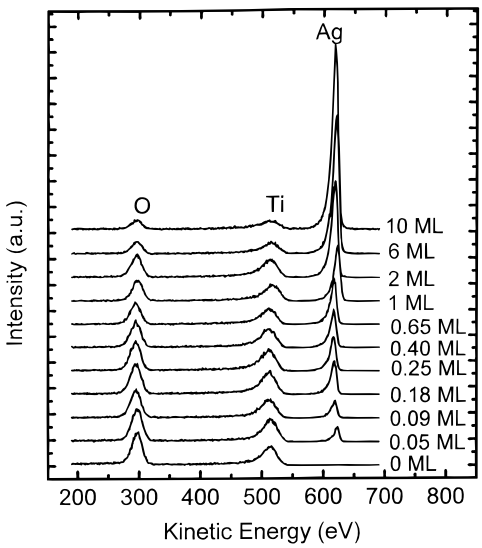

Figure 1. LEIS spectra of Ag/TiO_2(110) (1 × 1) at 300 K as a function of Ag exposure.

360) with an incident angle of ca. 30° from the surface normal. The LEIS data were acquired using a He^+ beam energy of 650 eV and an incident angle of 45° from the surface normal. To avoid surface damage, only one LEIS scan was collected for each spectrum.

The second UHV system (base pressure of 1×10^{-10} Torr) was equipped with STM (Omicron STM-1), XPS, AES, and LEED. In this chamber, the TiO_2 sample was mounted on a Ta sample holder, and the temperature measured with an optical pyrometer calibrated using a thermocouple. STM data were typically collected at sample biases of 1−2 V and tunneling currents of 0.5−2 nA. A more detailed experimental description can be found elsewhere.[32]

Results and Discussion

1. Ag/TiO_2 Growth Mode. There are three basic modes[2,4] for the growth of metal thin films on solids: layer-by-layer growth (Frank-van der Merwe, FM mode), three-dimensional (3D) cluster growth (Volmer−Weber, VW mode), and monolayer growth followed by three-dimensional growth (Stranski-Krastanov, SK mode). Generally, three-dimensional growth is expected for transition metal deposition onto TiO_2.[4] For Cu, LEIS studies[33,34] suggest 3D growth, whereas another study proposed a SK growth mode.[17] For Au deposited on TiO_2(110) at 300 K, two-dimensional growth was observed at fractional monolayer coverages, whereas 3D growth was apparent at higher Au coverages using STM and LEIS.[30,31]

In the present study, LEIS and STM were used to investigate the growth mode of Ag on TiO_2. LEIS is a highly surface sensitive technique for investigating surface composition. For layer-by-layer growth, a linear relationship between the LEIS peak area of the deposited metal and the metal exposure is anticipated, whereas a smooth, nonlinear relationship between these data are expected for a 3D growth mode. Figure 1 shows

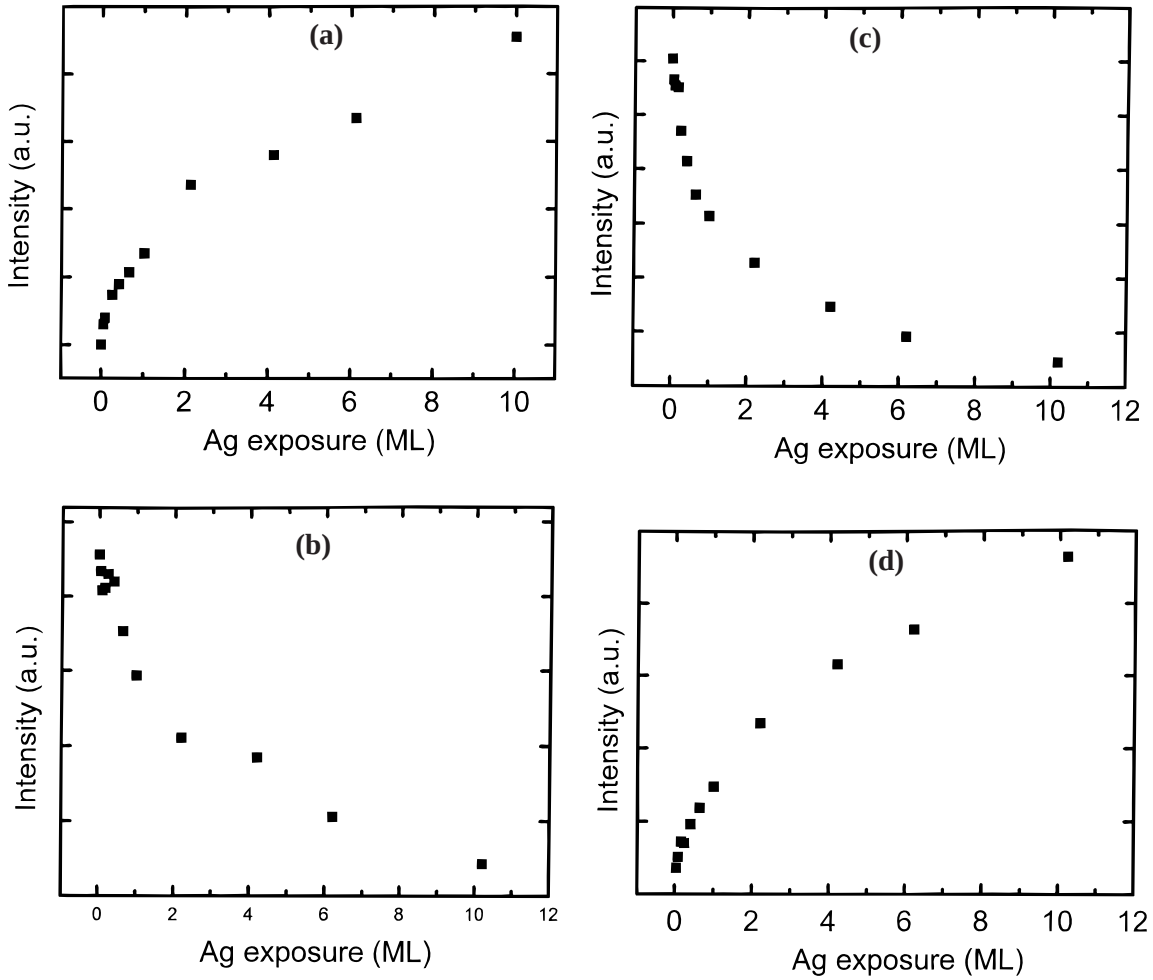

Figure 2. Integrated LEIS peak areas from Figure 1 as a function of Ag exposure on TiO_2(110) (1 × 1): Ag (a); Ti (b); O (c). Also shown is the Ag integrated LEIS peak area as a function of Ag exposure at 300 K on TiO_2(110) (1 × 2) (d).

LEIS spectra for increasing coverages of Ag on TiO_2(110) (1 × 1) at 300 K. The LEIS spectrum of the clean TiO_2 surface exhibits two features at 307 and 524 eV, corresponding to He^+ scattering from surface O and Ti sites, respectively. A feature at 629 eV, which appears following exposure of this surface to 0.05 ML Ag, is assigned to the He^+ scattered from surface Ag. This Ag feature increases with Ag coverage, while the Ti and O peaks decrease, although even after 10 ML Ag exposure, the O and Ti features are still evident. In Figure 2a, the Ag peak areas from the LEIS spectra in Figure 1 are shown as a function of Ag exposure. Similarly, parts b and c of Figure 2 show the Ti and O LEIS peak areas as a function of the Ag exposure. The nonlinearity in parts a−c of Figure 2 clearly indicates 3D growth of Ag on the TiO_2(110) (1 × 1) surface. Figure 2d shows the LEIS Ag peak areas as a function of Ag exposure on a TiO_2-(110) (1 × 2) surface at 300 K. The smooth, nonlinear relationship is consistent with the 3D growth of Ag on the (1 × 2) surface as well. The Ti and O plots also agree with a 3D growth mode. Comparing Ag growth on the (1 × 1) and (1 × 2) surfaces, the Ag/O and Ag/Ti LEIS peak area ratios from a (1 × 2) surface are larger than those from a (1 × 1) surface for the same Ag exposure. These results suggest that Ag disperses more completely on the (1 × 2) surface than on the (1 × 1) surface. The distance between Ti rows along the [001] direction of a (1 × 2) surface is significantly larger than that for the (1 × 1) surface. This increase in spacing together with the inherent roughness of the reconstructed surface likely contributes to the observed increase in Ag dispersion on TiO_2(110) (1 × 2).

Figure 3 shows STM images of clean TiO_2(110) (1 × 2), A and (1 × 1), B, surfaces. From the STM image in Figure 3a, (1 × 2) rows with a periodicity of 1.3 nm × 0.3 nm are evident. There are also several cluster structures on the surface with a diameter of ca. 1.0−1.5 nm. Since there was no contamination detectable either by XPS or AES, these cluster structures are believed to be either TiO_2 or Ti_2O_3. Compared to the (1 × 2) surface, the (1 × 1) surface in Figure 3b has a larger number of terraces and fewer isolated cluster structures than TiO_2(110) (1 × 1). The smaller terraces of the (1 × 1) surface are anticipated since this surface is prepared at a significantly lower annealing temperature than the (1 × 2) surface.

An STM image of a TiO_2(110) (1 × 1) surface exposed to 0.05 ML Ag is shown in Figure 4. The clusters are 2−3.5 nm in diameter with heights of 0.6−0.7 nm, corresponding to approximately two atomic Ag layers. The 3D clusters and patches of bare substrate indicate a 3D growth mode as previously reported[30] and in agreement with the LEIS results discussed above. Parts a, b, and c of Figure 5 show STM images of 0.05, 0.5, and 2.0 ML Ag on TiO_2(110) (1 × 2) surface, respectively. Bare substrate patches can be seen in all three images. At 0.05 ML, the diameters of the Ag clusters are 2−3 nm, with heights of 0.5−0.6 nm, consistent with approximately two Ag atomic layers. With increasing Ag exposure, the cluster diameters and heights increase. At 0.5 ML, the cluster diameters are 2.5−4 nm, with a height of 0.6−1 nm. At 2 ML, the cluster diameters are 3−5 nm, with heights of 0.8−1.7 nm. These results are very consistent with a 3D interpretation for the growth mode of Ag on the TiO_2(110) (1 × 2) surface at 300 K.

Generally, on both surfaces, Ag prefers to nucleate at step edge defect sites rather than the flat terrace defect sites. Also, for a given exposure, the Ag cluster density on the (1 × 2) surface is larger, and the cluster diameter and height is smaller, than on the (1 × 1) surface. For example, at a 0.5 ML Ag exposure, the Ag cluster heights on a (1 × 1) surface are 1.0−1.5 nm,[30] while the heights on a (1 × 2) surface are 0.8−1 nm.

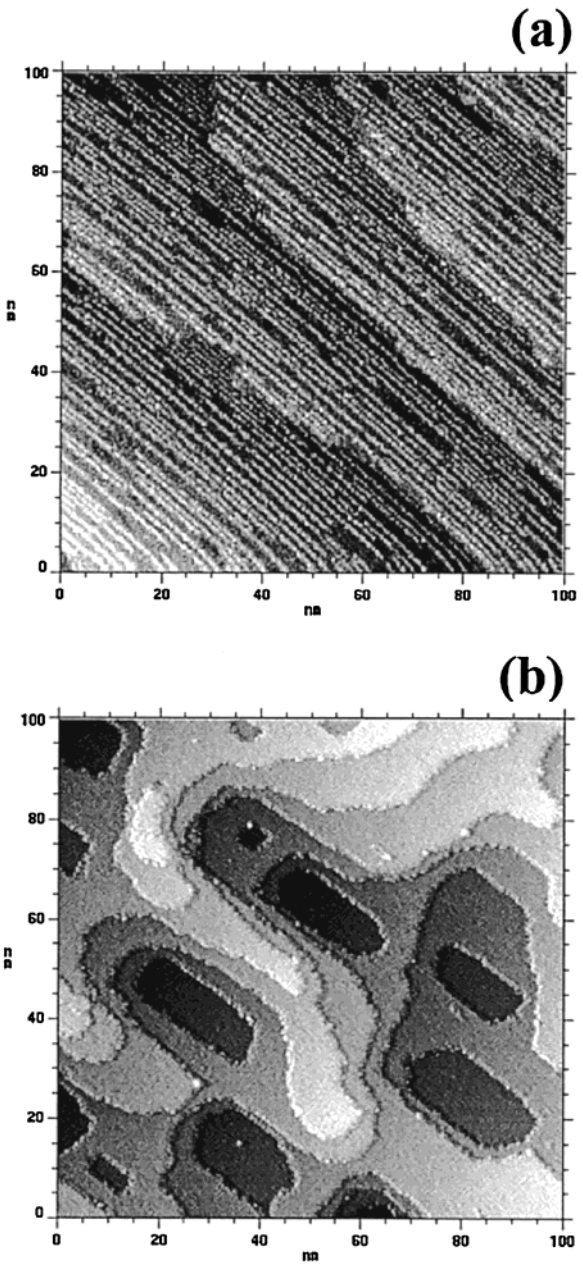

Figure 3. Constant current topography (CCT) STM images of TiO_2-(110) (1 × 2) (100 × 100 Å, 2 V, 1 nA) (a) and (1 × 1) (100 × 100 Å, 2 V, 2 nA) (b).

Similarly, the cluster diameter on a (1 × 1) surface are 3.5−4 nm,[30] while the cluster diameters on a (1 × 2) surface are 2.5−4 nm. These results are consistent with the LEIS results and suggest a higher dispersion of Ag on the (1 × 2) surface compared with the (1 × 1) surface.

2. Ag/TiO_2 Electronic Properties: An XPS Investigation. XPS is an excellent technique for studying the chemical interactions between metal particles and metal oxide substrates in that the core level binding energy shifts give direct information about the metal and substrate electronic properties. Figure 6a shows Ag 3d core level photoemission spectra as a function of Ag exposure on a TiO_2(110) (1 × 1) surface at 100 K. The Ag 3d peaks shift to higher binding energy as the Ag coverage decreases. For example, the Ag $3d_{5/2}$ peak shifts by +1.2 eV from the "bulk" value as the coverage decreases to 0.05 ML (2.0−3.5 nm from STM study). From the STM data, it has been established that the Ag cluster size decreases as the Ag coverage

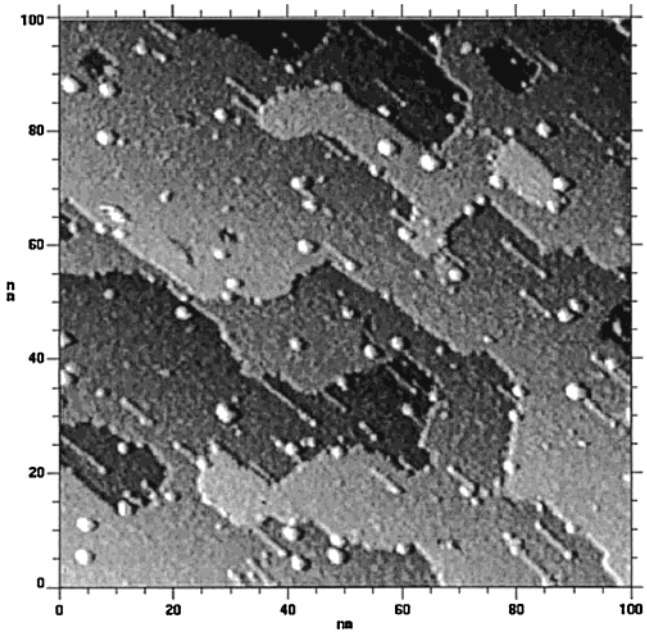

Figure 4. CCT STM images of 0.05 ML Ag exposure on TiO_2(110) (1 × 1) surface (100 × 100 Å, 1.5 V, 0.5 nA).

decreases; hence, the Ag 3d binding energy shifts reflect the decrease in cluster size. Binding energy shifts for metal clusters deposited onto certain conductive substrates can be attributed to initial state[35−42] and/or final state effects.[26,31,40,43,44] Final state effects arise from screening of the core level hole created by photoemission, i.e., electrons relax to screen the hole, resulting in a photoemitted electron with a higher kinetic energy and therefore lower binding energy. If a given cluster is small enough that the screening is significantly less than that of the bulk, then the result is a shift of the photoemission peaks to higher binding energy. Initial state effects may also contribute to an observed binding energy shift through (1) an interfacial chemical reaction, (2) a binding energy difference between surface and bulk atoms, or (3) metal cluster nucleation on different defect sites.

Simultaneously with the Ag 3d spectra, photoemission spectra from the Ti 2p and O 1s regions were acquired. The intensity of the Ti 2p peak in Figure 6b decreases with increasing Ag coverage; however, there is no obvious shift of the Ti $2p_{3/2}$ peak maximum at 459.1 eV (the variation of the peak position is about 0.2 eV). A Ti^{3+} shoulder at lower binding energy position is not evident, nor is there a peak shift for the O 1s binding energy feature. If metal clusters were to react with an oxide substrate, the resulting charge transfer would lead to an oxidation state change, i.e., a shift in the Ti 2p and O 1s core level states. That there are no significant shifts or new oxidation states observed for either the Ti 2p or the O 1s peaks suggests little chemical interaction at the Ag/TiO_2 interface. The lack of a strong interfacial interaction between Ag and TiO_2 and the smaller core level binding energy shift of the Ag 3d feature upon oxidation[25,45,46] suggests a minor role of initial state contributions.

Binding energy differences between surface atoms and bulk atoms can be significant because the metal atoms at the perimeter of clusters are less coordinated compared with the atoms inside the clusters (bulklike atoms). The binding energy differences between the surface and bulk can be either positive or negative, depending upon the metal. According to previous work,[36] the 3d binding energy of Ag surface atoms shifts to a value of ca. 0.08 eV less than the corresponding bulk value. The results presented here show a positive binding energy shift

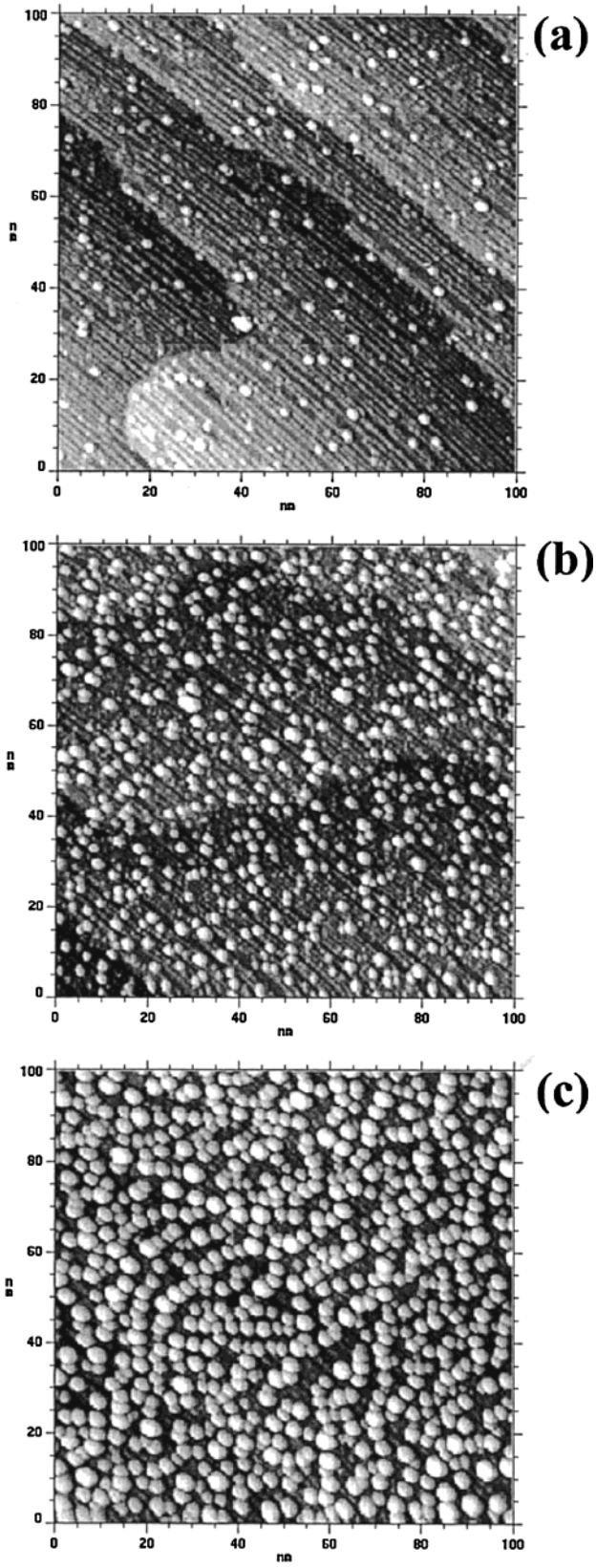

Figure 5. CCT STM images of Ag on TiO_2(110) (1 × 2): (a) 0.05 ML; (b) 0.5 ML; (c) 2 ML (100 × 100 Å, 2 V, 0.5 nA).

as the cluster size decreases, i.e., as the relative population of surface atoms increases. Therefore, the binding energy increase cannot be due entirely to the difference in binding energies between surface and bulk atoms.

The STM results show that the Ag clusters prefer to grow on surface step-edge defects rather than flat terrace defects. The

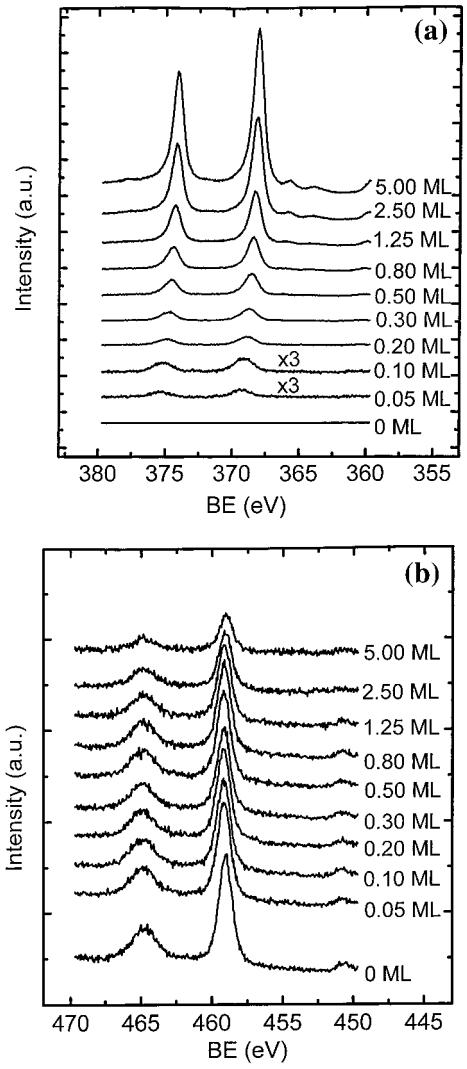

Figure 6. Ag 3d (a) and Ti 2p (b) XPS spectra as a function of Ag exposure on TiO_2(110) (1 × 1).

growth of Ag clusters on various defects (F centers or V centers) may lead to differences in the Ag binding energies. At low Ag coverages, this interfacial effect will dominate the photoemission features. However, the effect is not easily detected with increasing Ag coverage, especially for a 3D growth mode, because of the small free mean path of the Ag photoelectrons. The various binding states arising from these effects can also lead to a broadening (heterogeneous) of the photoemission peak, as will be discussed in the following section. In conclusion, the higher Ag binding energy shifts can be attributed to final state effects and/or cluster nucleation onto different surface sites (initial state effects).

The Ag $3d_{5/2}$ fwhm's of Figure 6a, plotted as a function of the Ag exposure in Figure 7, show that the peak width becomes broader with decreasing Ag coverage. This broadening can result from the three initial state effects mentioned above; however, reasoning as above, the first two contributions can be ruled out. That is, heterogeneous nucleation is likely the major contributing factor to the fwhm peak broadening, although the inherent size distribution of the Ag clusters could also play a role. For example, final state screening occurs to varying degrees for Ag clusters of different sizes, leading to a distribution of binding energies, i.e., a broadened photoemission peak.

The Ag $3d_{5/2}$ core level binding energy as a function of Ag exposure on TiO_2(110) (1 × 1) and (1 × 2) surfaces at 100 and

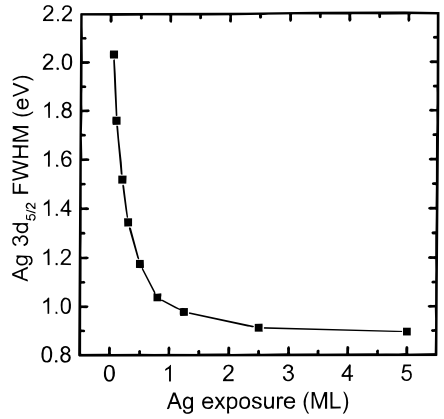

Figure 7. The Ag $3d_{5/2}$ full width at half-maximum (fwhm) from Figure 6a as a function of Ag exposure on TiO_2(110) (1 × 1).

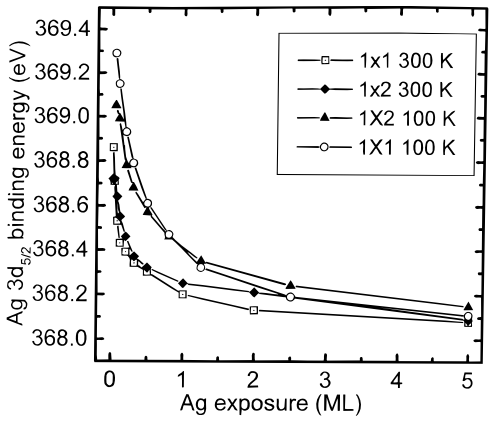

Figure 8. XPS Ag $3d_{5/2}$ core level shift as a function of Ag exposure on TiO_2 (110) (1 × 1) and (1 × 2) at 100 and 300 K. The upper open circles and solid triangles represent results of Ag deposited on TiO_2 (110) (1 × 1) and (1 × 2), respectively, at 100 K. The open square and solid diamond lines represent the results of Ag deposited on TiO_2-(110) (1 × 1) and (1 × 2), respectively, at 300 K.

300 K, respectively, are presented in Figure 8. After large exposures, the Ag 3d binding energies reflect the presence of metallic Ag. The binding energy trends are similar on both surfaces and at both temperatures; that is, at lower coverages, i.e., smaller cluster sizes, the binding energy shifts to higher values. At 100 K, the binding energy shifts are more gradual at the initial fractional coverages than at 300 K. In addition, for the same given Ag exposure, the binding energy at 100 K is higher than that at 300 K; however, this difference becomes much less as the coverage increases. The binding energy finally converges to that of metallic Ag after the addition of ca. 5 ML Ag exposure. Deposition at 100 K results in a binding energy shift of ∼1.0 eV over the entire coverage range. However, at 300 K, the shifts are approximately 0.7 and 0.6 eV for the (1 × 1) and (1 × 2) surfaces, respectively. These results indicate that Ag forms larger clusters with increasing coverage and that the larger clusters have more metallic electronic character. The larger overall peak shift and reduced binding energy increase at lower temperature suggest the nucleation of smaller clusters at lower temperatures. Ag deposition on the (1 × 1) and (1 × 2) surfaces results in clusters that have similar electronic properties.

Figure 9a shows the XPS valence band spectra of the TiO_2 (110) (1 × 1) surface as a function of Ag exposure at 100 K. The bottom spectrum shows the O 2p structure from the clean TiO_2 substrate, which ranges from ∼3.2 to 9.6 eV.[9,10,13,47,48] With increasing Ag exposure, the Ag 4d band dominates the

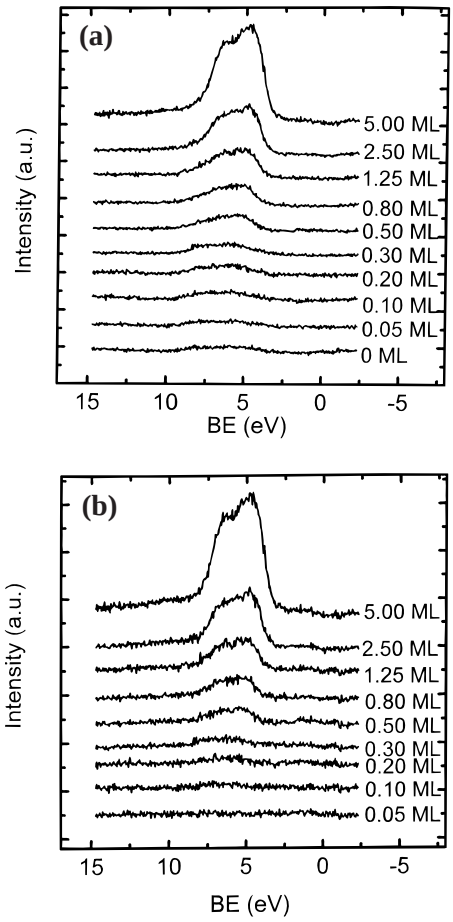

Figure 9. X-ray induced valence band spectra of (a) Ag/TiO_2(110) (1 × 1) at 100 K and (b) the spectra from (a) with the TiO_2 valence band subtracted.

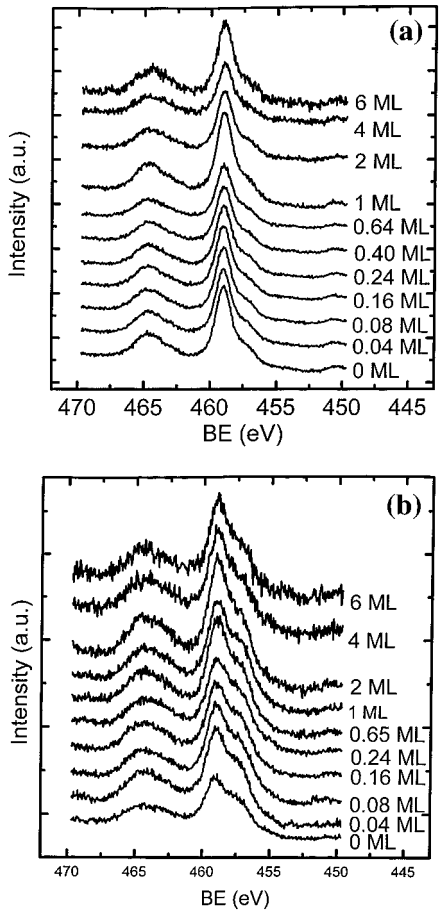

Figure 10. XPS Ag 3d of Ag on (a) lightly Ar ion-bombarded and (b) heavily Ar ion-bombarded TiO_2(110) (1 × 1) at 300 K.

spectra. In the Ag 4d spectra of Figure 9b, the TiO_2 background spectrum has been subtracted. Because of the relatively low Ag 4d X-ray cross section, the features are poorly defined for Ag exposures less than 0.2 ML; however, for Ag coverages from 0.2 to 5 ML, the center of the valence band shifts from 6.5 to 5.5 eV. The magnitude of this shift is consistent with the Ag 3d core level binding energy shift cited above (∼1 eV). The absence of a well-defined Fermi level even for the relatively high exposures is noteworthy and likely due to the low X-ray cross section of the Ag sp band. From Figure 9b, the Ag 4d bandwidth, ranging from 3 to 8.0 eV at 5 ML Ag exposure, is significantly narrower than that of the O 2p bandwidth, with a prominent feature at ∼4.8 eV, and a second feature centered at 6.3 eV. From previous studies,[26,44] the features at 4.8 and 6.3 eV can be attributed to metallic Ag. At Ag coverages <0.5 ML, the peak width is somewhat narrower with a less-pronounced high binding energy shoulder. At 0.5 ML, the feature at ∼5.0 eV increases in intensity. These results are consistent with a recent scanning tunneling spectroscopy (STS) study[49] that showed a metal-to-nonmetal transition between 0.5 and 1.0 ML Ag exposure.

3. Effects of Ion Bombardment to Nucleation and Growth of Ag/TiO_2. Ion bombardment is well-known to preferentially remove oxygen from TiO_2 surfaces, resulting in the creation of Ti^{3+} states within the surface and near surface regions. These states, which can be detected via XPS, can serve as nucleation sites for metal clusters. Studying the interaction of metal clusters with these defect states can be useful in determining the extent of interfacial reaction for a particular metal/oxide system. Therefore, the deposition of Ag onto ion-bombarded TiO_2 surfaces was studied using XPS and LEIS. A "lightly" Ar ion-bombarded surface was prepared using 1 keV Ar^+ and a sputter current of 0.4 μA for 1.5 min, while a "heavily" Ar ion-bombarded surface was prepared using 2 keV Ar^+ and a sputter current of 0.8 μA for 4 min. Figure 10a shows Ti 2p XPS spectra as a function of Ag exposure at 300 K on a lightly ion-bombarded TiO_2(110) (1 × 1) surface. The clean surface is characterized by a Ti 2p region that has the typical Ti^{4+} $2p_{3/2}$ peak at 459.0 eV and an second shoulder feature at ∼457.3 eV assigned to the Ti^{3+} states created by ion-bombardment.[50,51] After exposures up to 6 ML, the Ti^{3+} shoulder remains unchanged. Figure 10b shows Ti 2p XPS spectra as a function of Ag exposure at 300 K on a heavily ion-bombarded TiO_2-(110) (1 × 1) surface. The clean surface is characterized by a much larger Ti^{3+} feature (which also may include Ti^{2+} states) than is seen for a lightly ion-bombarded surface. After Ag exposures up to 6 ML, no obvious peak shift or shape change is apparent. Previous studies[40,50,52] of both Rh and Pt indicate 3D metal growth on TiO_2(110) surfaces. Specifically, for Rh and Pt deposited onto an Ar ion-bombarded TiO_2 surface, the reduced Ti^{3+} state is oxidized back to the Ti^{4+} state.[48,50] In the present studies, there is no evidence that Ti^{3+} is oxidized upon the deposition of Ag onto TiO_2(110) (1 × 1) and (1 × 2) surfaces, suggesting that there is no strong interaction between Ag clusters and reduced Ti^{3+} or Ti^{2+} states.

In parts a, b, and c of Figure 11, Ag $3d_{5/2}$ binding energies are shown as a function of Ag exposure at 300 K on well ordered, lightly sputtered, and heavily sputtered (1 × 1) surfaces, respectively. The Ag $3d_{5/2}$ binding energy shifts of the stoichiometric (Figure 11a), the lightly sputtered (Figure 11b), and the heavily sputtered (Figure 11c) surfaces all display the same

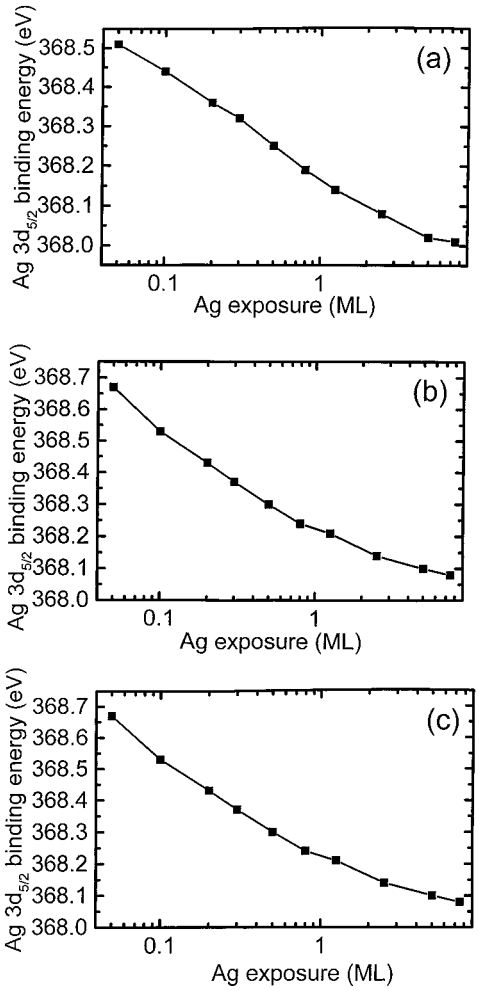

Figure 11. XPS Ag 3d core level shift from Ag clusters on (a) well ordered, (b) lightly Ar ion-bombarded, and (c) heavily Ar ion-bombarded $TiO_2(110)$ (1×1) surfaces as a function of Ag exposure at 300 K.

trend. It is noteworthy that the shifts do not decrease at a significantly lower rate than was observed for Rh/TiO_2.[50] Noting that the Ag 3d binding energy is an indicator of cluster size, these data suggest that the Ag growth mode varies little on the various sputtered surfaces. LEIS experiments also showed similar results for all three sputter-treated surfaces, consistent with similar metal growth modes of each. Parallel studies of Ag grown on sputtered (1×2) surfaces yielded identical results.

4. Effect of Annealing on Ag growth on TiO_2. An exposure of 0.75 ML Ag on a well-ordered (1×1) surface at 100 K was studied by LEIS as a function of the annealing temperature. In Figure 12, the LEIS peak area ratios of Ag/Ti and Ag/O are shown as a function of the annealing temperature. From 100 to 300 K, the Ag/Ti and Ag/O ratios decrease rapidly, then remain essentially constant as the annealing temperature increases from 300 to 600 K. Between 600 and 900 K, the ratios decrease, but at a slower rate than for the lower temperature annealing. Above 900 K, the Ag clusters begin evaporating from the surface; by 1060 K, no Ag is detected by XPS. Because LEIS is sensitive to the topmost surface layer, the elemental peak ratios can be related directly to the surface area stoichiometry. Thus, the decreasing Ag/Ti and Ag/O ratios with annealing temperature indicate that the Ag clusters are sintering, and this is particularly obvious within the low-temperature region (100−300 K). At higher temperatures, the Ag clusters agglomerate until that temperature at which Ag sublimation begins.

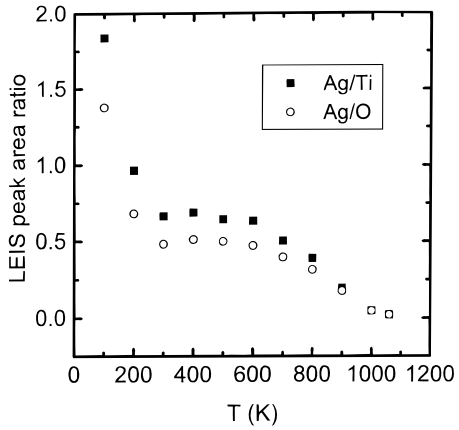

Figure 12. Ag/Ti and Ag/O LEIS peak area ratios as a function of temperature for 0.75 ML Ag on $TiO_2(110)$ (1×1) surface.

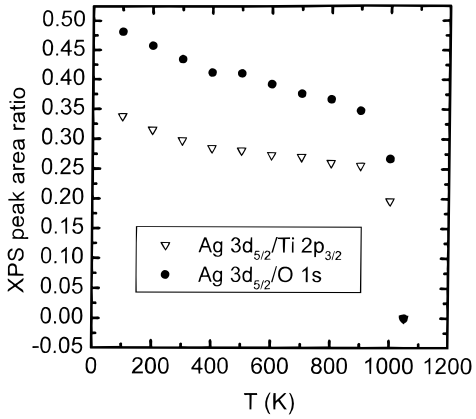

Figure 13. Integrated XPS Ag $3d_{5/2}$/Ti 2p and Ag $3d_{5/2}$/O 1s XPS peak area ratios of 0.75 ML Ag on $TiO_2(110)$ (1×1) as a function of annealing temperature between annealings. The spectra were collected at 100 K.

The data in Figure 8 show the effect of the nucleation temperature on the Ag cluster growth. Deposition at 300 K results in Ag clusters that are characterized by lower Ag $3d_{5/2}$ binding energies than those Ag clusters deposited at 100 K at identical Ag exposures. Further XPS investigations of the nucleation of a 0.75 ML Ag exposure on the (1×1) surface at 100 K as a function of annealing temperatures in 100 K increments are shown in Figure 13. Here the Ag $3d_{5/2}$/Ti $2p_{3/2}$ and Ag $3d_{5/2}$/O 1s peak area ratios are shown as a function of the annealing temperature. Since XPS is less surface sensitive than LEIS, the ratios decrease to a lesser extent than for the LEIS data acquired within the same temperature regime. Nevertheless, it is still very evident that the Ag clusters are sintering as the annealing temperature increases, particularly obvious within the temperature region 100−300 K. This trend of decreasing peak area ratios with increasing temperature is consistent with the LEIS results.

The effect of annealing on higher Ag coverages was also studied, with results very similar to those shown in Figure 13. Parts a and b of Figure 14 show the Ag $3d_{5/2}$ binding energy and fwhm, respectively, collected simulataneously with the data in Figure 13. The core level data of Figure 14a shifts to lower values with increasing temperature while the fwhm decreases, as shown in Figure 14b. The reduction in binding energy and fwhm with increasing annealing temperature are consistent with cluster sintering. Between 100 and 300 K, the binding energy shift and fwhm decrease are more significant than the corresponding decrease of those values between 400 and 800 K,

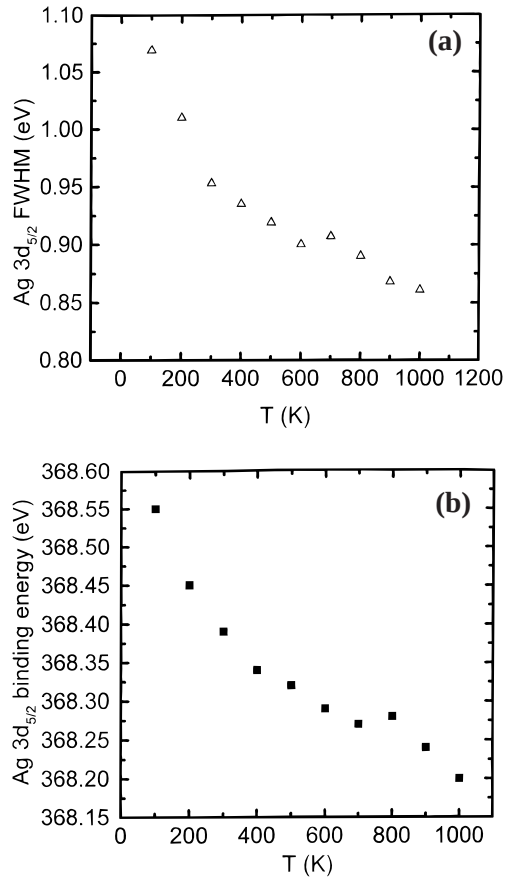

Figure 14. XPS Ag $3d_{5/2}$ core level binding energy (a) and fwhm (b) of 0.75 ML Ag on TiO_2(110) (1 × 1) surface as a function of annealing temperature between annealings. The spectra were collected at 100 K.

consistent with the data of Figures 12 and 13, where the sintering rates are more rapid in the low-temperature region. During the annealing experiments, the Ti 2p and O 1s peak widths also slightly broaden (not shown); at temperatures of >1000 K, a small Ti 2p shoulder at lower binding energy appears. Previous studies[31,53,54] of stoichiometric TiO_2 showed that annealing reduces the surface; therefore, the Ti 2p and O 1s broadening is attributed to a temperature-induced reduction.

Conclusions

Silver growth on TiO_2(110) (1 × 1) and (1 × 2) surfaces at 300 K was studied by XPS, LEIS, and STM, and the growth was shown to be 3D. The Ag 3d binding energy shift and peak broadening are attributed to a combination of heterogeneous broadening and final state screening effects. The Ag clusters are stable on the TiO_2 surface and no significant chemical interaction between Ag and TiO_2 is observed on well-ordered, sputtered, or annealed surfaces. On the other hand, the effect of annealing on the sintering of Ag clusters is evident on TiO_2. In general, both the TiO_2(110) (1 × 1) and (1 × 2) surfaces show very similar results with respect to nucleation and growth of Ag clusters.

Acknowledgment. We acknowledge with pleasure the support of this work by the Department of Energy, Office of Basic Energy Sciences, Division of Chemical Sciences, the Dow Chemical Company, and the Robert A. Welch Foundation. We also thank Dr. Paul Bagus for the discussion of the results.

References and Notes

(1) Campbell, C. T. *Surf. Sci. Rep.* **1997**, *27*, 1.
(2) Henrich, V. E.; Cox, P. A. *The Surface Science of Metal Oxides*; Cambridge University Press: Cambridge, 1994.
(3) Goodman, D. W. *Surf. Rev. Lett.* **1995**, *2*, 9.
(4) Persaud, R.; Madey, T. E. *The Chemical Physics of Solid Surfaces and Heterogeneous Catalysis*; King, D. A., Woodruff, D. P., Eds.; Elsevier: Amsterdam, 1997; Vol. 8, p 407.
(5) Lad, R. J. *Surf. Rev. Lett.* **1995**, *2*, 109.
(6) Freund, H.-J.; Bunsenges, B. *Phys. Chem.* **1985**, *99*, 1261.
(7) St. Clair, T. P.; Goodman, D. W. *Top. Catal.*, in press.
(8) Diebold, U.; Pan, J.-M.; Madey, T. E. *Surf. Sci.* **1995**, *331*, 845.
(9) Henrich, V. E.; Kurtz, R. L. *Phys. Rev. B* **1981**, *23*, 6280.
(10) Tait, R. H.; Kasowski, R. V. *Phys. Rev. B* **1979**, *20*, 5178.
(11) Göpel, W. *Surf. Sci.* **1984**, *139*, 333.
(12) Göpel, W.; Rocker, G.; Feierabend, R. *Phys. Rev. B* **1983**, *28*, 3427.
(13) Guo, Q.; Lee, S.; Goodman, D. W. *Surf. Sci.* **1999**, *437*, 38.
(14) Sadeghi, H. R.; Henrich, V. E. *J. Catal.* **1988**, *109*, 1.
(15) Cox, P. A.; Egdell, R. G.; Eriksen, S.; Flavell, W. R. *J. Electron Spectrosc.* **1986**, *39*, 117.
(16) Rocker, G.; Schaefer, J. A.; Göpel, W. *Phys. Rev. B* **1984**, *30*, 3704.
(17) Møller, P. J.; Wu, M.-C. *Surf. Sci.* **1989**, *224*, 265.
(18) Kao, C. C.; Tsai, S. C.; Bahl, M. K.; Chung, Y. W.; Lo, W. J. *Surf. Sci.* **1980**, *95*, 1.
(19) Chung, Y. W.; Lo, W. J.; Somorjai, G. A. *Surf. Sci.* **1977**, *64*, 588.
(20) Cocks, I. D.; Guo, Q.; Williams, E. M. *Surf. Sci.* **1997**, *390*, 119.
(21) Onishi, H.; Iwasawa, Y. *Surf. Sci.* **1994**, *313*, L783.
(22) Novak, D.; Garfunkel, E.; Gustafsson, T. *Phy. Rev. B* **1994**, *50*, 5000.
(23) Tanner, R. E.; Castell, M. R.; Briggs, G. A. D. *Surf. Sci.* **1998**, *412/413*, 672.
(24) Fischer, S.; Munz, A. W.; Schierbaum, K.-D.; Göpel, W. *Surf. Sci.* **1995**, *337*, 17.
(25) Bukhtiyarov, V. I.; Prosvirin, I. P.; Kvon, R. I.; Goncharova, S. N.; Bal'zhinimaev, B. S. *J. Chem. Soc., Faraday Trans.* **1997**, *93*, 2323.
(26) Rodriguez, J. A.; Kuhn, M.; Hrbek, J. *J. Phys. Chem.* **1996**, *100*, 18240.
(27) VanCampen, D. G.; Herbek, J. *J. Phys. Chem.* **1995**, *99*, 16389.
(28) Martin, D.; Creuzet, F.; Jupille, J.; Borensztein, Y.; Gadenne, P. *Surf. Sci.* **1997**, *377*, 958.
(29) Abriou, D.; Gasgnot, D.; Jupille, J.; Creuzet, F. *Surf. Rev. Lett.* **1998**, *5*, 387.
(30) Lai, X.; St. Clair, T. P.; Valden, M.; Goodman, D. W. *Prog. Surf. Sci.* **1998**, *59*, 25.
(31) Zhang, L.; Persaud, R.; Madey, T. E. *Phys. Rev. B* **1997**, *56*, 10549.
(32) Xu, C.; Lai, X.; Zajac, G. W.; Goodman, D. W. *Phys. Rev. B* **1997**, *56*, 13464.
(33) Diebold, U.; Pan, J.-M.; Madey, T. E. *Phys. Rev. B* **1993**, *47*, 3868.
(34) Pan, J.-M.; Maschhoff, B. L.; Diebold, U.; Madey, T. E. *Surf. Sci.* **1993**, *291*, 381.
(35) Eastman, D. E.; Himpsel, F. J.; van der Veen, J. F. *J. Vac. Sci. Technol.* **1982**, *20*, 609.
(36) Citrin, P. H.; Wertheim, G. K. *Phy. Rev. Lett.* **1978**, *41*, 1425.
(37) van der Veen, J. F.; Heimann, P.; Himpsel, F. J.; Eastman, D. E. *Solid State Commun.* **1981**, *37*, 555.
(38) Bagus, P. S.; Brundle, C. R.; Pacchioni, G.; Parmigiani, F. *Surf. Sci. Rep.* **1993**, *19*, 265.
(39) Bagus, P. S.; Coulbaugh, D.; Kowalczyk, S. P.; Pacchioni, G.; Parmigiani, F. *J. Electron Spectrosc.* **1990**, *51*, 69.
(40) Steinrück, H.-P.; Pesty, F.; Zhang, L.; Madey, T. E. *Phys. Rev. B* **1995**, *51*, 2427.
(41) Egelhoff, W. F. *Surf. Sci. Rep.* **1987**, *6*, 253.
(42) Rainer, D. R.; Goodman, D. W. *J. Mol. Catal. A: Chem.* **1998**, *131*, 259.
(43) Citirin, P. H.; Wertheim, G. K. *Phys. Rev. B* **1983**, *27*, 3176.
(44) Hüfner, S.; Wertheim, G. K.; Wernick, J. H. *Phys. Rev. B* **1973**, *8*, 4511.
(45) Schön, G. *Acta Chem. Scand.* **1973**, *27*, 2623.
(46) Hammond, J. S.; Gaarenstroom, S. W.; Winograd, N. *Anal. Chem.* **1975**, *47*, 2193.
(47) Fischer, S.; Schierbaum, K.-D.; Göpel, W. *Vacuum* **1997**, *48*, 601.
(48) Schierbaum, K.-D.; Fischer, S.; Torquemada, M. C.; de Segovia, J. L.; Román, E.; Martin-Gago, J. A. *Surf. Sci.* **1996**, *345*, 261.
(49) St. Clair, T. P.; Lai, X.; Luo, K.; Goodman, D. W. In preparation.
(50) Berkó, A.; Ulrych, I.; Prince, K. C. *J. Phys. Chem. B* **1998**, *102*, 3379.
(51) Mayer, J. T.; Diebold, U.; Madey, T. E. *J. Electron. Spectrosc.* **1995**, *73*, 1.
(52) Berkó, A.; Ménesi, G.; Solymosi, F. *Surf. Sci.* **1997**, *372*, 202.
(53) Pan, J. M.; Maschhoff, B. L.; Diebold, U.; Madey, T. E. *J. Vac. Sci. Technol. A* **1992**, *10*, 2470.
(54) Oh, W. S.; Xu, C.; Kim, D. Y.; Goodman, D. W. *J. Vac. Sci. Technol. A* **1997**, *15*, 1710.